Rational design of true monomeric and bright photoactivatable fluorescent proteins

Mingshu Zhang[1,2,6], Hao Chang[1,3,6], Yongdeng Zhang[1,4,6], Junwei Yu[1,4], Lijie Wu[1], Wei Ji[1], Juanjuan Chen[5], Bei Liu[1,4], Jingze Lu[1], Yingfang Liu[1], Junlong Zhang[5], Pingyong Xu[1] & Tao Xu[1,4]

Monomeric (m)Eos2 is an engineered photoactivatable fluorescent protein widely used for super-resolution microscopy. We show that mEos2 forms oligomers at high concentrations and forms aggregates when labeling membrane proteins, limiting its application as a fusion partner. We solved the crystal structure of tetrameric mEos2 and rationally designed improved versions, mEos3.1 and mEos3.2, that are truly monomeric, are brighter, mature faster and exhibit higher photon budget and label density.

Recently developed super-resolution imaging techniques, such as photoactivated localization microscopy (PALM)[1], fluorescence PALM (FPALM)[2] and stochastic optical reconstruction microscopy (STORM)[3], collectively referred to here as (F)PALM/STORM, are revolutionizing the study of cellular ultrastructures at unprecedented resolutions. In many cases, genetically encoded molecules that can be photoswitched are preferred for (F)PALM/STORM. The performance of super-resolution imaging relies heavily on the characteristics of photoactivatable fluorescent proteins (PAFPs). Key properties that determine the practical use of PAFPs include (but are not limited to) size, brightness, maturation rate, oligomeric nature, pH stability and photon budget after switching. Also, although often neglected, the label density limits the effective spatial resolution in all super-resolution fluorescence microscopy[4].

EosFP[5] is one of the best overall performing green-to-red PAFPs because it provides the highest photon output of all known PAFPs[6]. To overcome the inherent tetrameric nature of EosFP, several monomeric forms such as mEosFP, tandem dimer (td)EosFP and mEos2 have been developed[5,7,8]. Of these, mEos2 and tdEosFP are preferable to mEosFP because the chromophore of mEosFP does not mature at 37 °C, which limits its use to non-mammalian cells. tdEosFP has been reported to cause incorrect localization for many standard targets such as tubulin, histones and intermediate filaments[7], probably because of its large size. mEos2 alleviated the maturation problems of EosFP and has yielded the best localization precision achieved thus far for a PAFP (~10 nm in one dimension)[7].

However, mEos2 tends to form dimers and higher-order oligomers at high concentrations[7,9] (**Supplementary Fig. 1**). This problem is exacerbated when mEos2 is used to label membrane proteins, for which a very high local concentration can be reached owing to confined two-dimensional movement and limited rotation[10]. Indeed, we found that mEos2 invariably caused incorrect intracellular aggregates when fused to membrane proteins, including a subunit of the calcium release–activated calcium (CRAC) channel (Orai1) (**Fig. 1a**), G protein–coupled receptor GRM4 and glucose transporter 4 (GLUT4) (**Supplementary Fig. 2**). These results suggest that mEos2 is not a true monomer, and the weak oligomerization tendency of mEos2 may limit its use as a fusion partner in living cells.

To generate a true monomeric PAFP with optimal optical characteristics, we first investigated the molecular basis underlying the oligomerization of mEos2 by solving its crystal structure. We obtained the green-state mEos2 crystal in the absence of light and determined the structure at 2.2 Å (**Supplementary Table 1**). mEos2 exhibited a well-defined tetramer structure (**Fig. 1b**). It consisted of four classical β cans, which contact one another to form two types of interfaces.

By carefully examining the residue–residue interactions at two interfaces, we found three key residues that may participate in the oligomerization of mEos2. At the A–B interface, the hydrophobic side chain of Ile102 formed hydrophobic interactions with the side chains of Ile100 and Ile102; two Tyr121 residues facing each other also formed strong hydrophobic interactions (**Fig. 1c**). At the A–C interface, we found that the hydroxyl group of Tyr189 made a water-mediated hydrogen bond with the backbone oxygen atom of His158 (**Fig. 1d**). From these results, we reasoned that Ile102 and Tyr121 at the A–B interface and Tyr189 at the A–C interface are critical for the formation of the tetramer. Combined with a sequence alignment between mEos2 and other commonly used PAFPs (**Supplementary Fig. 3**), we speculated that mutations of Ile102 to asparagine (a similar mutation converts 22G into its monomer counterpart, Dronpa[11]), Tyr121 to a charged residue, such as arginine or lysine, and Tyr189 to alanine[12] would break the β-can–β-can interactions in the tetramer. As expected,
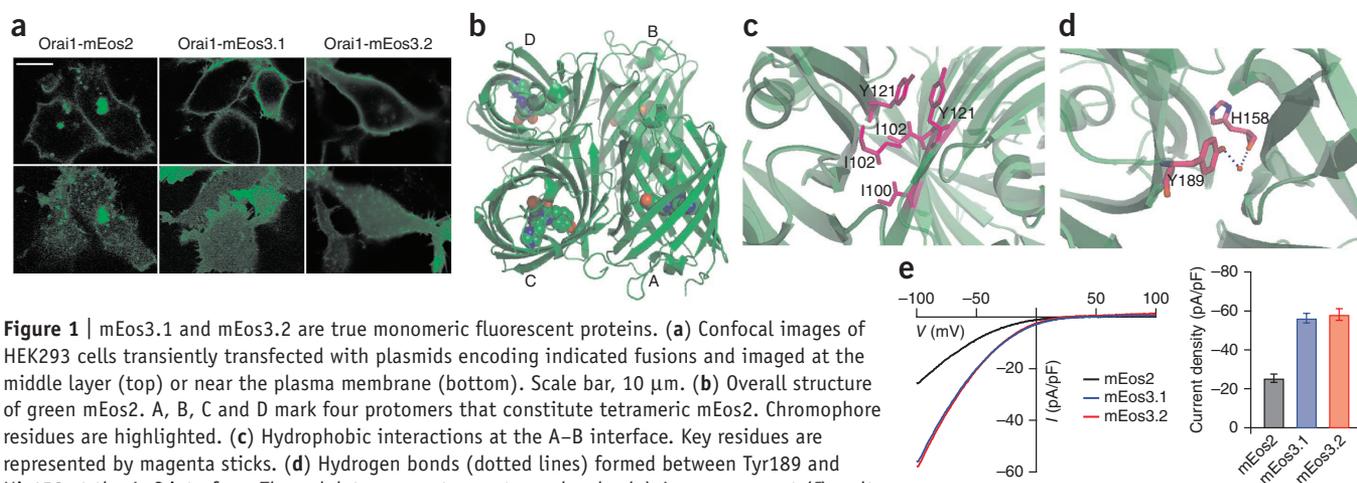
Figure 1 | mEos3.1 and mEos3.2 are true monomeric fluorescent proteins. (**a**) Confocal images of HEK293 cells transiently transfected with plasmids encoding indicated fusions and imaged at the middle layer (top) or near the plasma membrane (bottom). Scale bar, 10 μm. (**b**) Overall structure of green mEos2. A, B, C and D mark four protomers that constitute tetrameric mEos2. Chromophore residues are highlighted. (**c**) Hydrophobic interactions at the A–B interface. Key residues are represented by magenta sticks. (**d**) Hydrogen bonds (dotted lines) formed between Tyr189 and His158 at the A–C interface. The red dot represents a water molecule. (**e**) Average current (I)–voltage (V) relationships of leak-subtracted CRAC currents extracted from representative HEK293 cells expressing both STIM1-mKO and mEos2-, mEos3.1- or mEos3.2-labeled Orai1 (left) and average of peak current densities at −100 mV in cells expressing the indicated proteins in fusion (right). The average peak current densities of mEos3.1 ($P = 1.17 \times 10^{-7}$) and mEos3.2 ($P = 5.18 \times 10^{-8}$) are significantly larger than that of mEos2. P values were determined by Student's t-test; $n = 9$. Error bars, s.e.m.

the I102N mutant had the best monomeric behavior among all mutants and exhibited modest fluorescence. The Tyr121 mutations also reduced oligomerization to varying extent but lowered brightness. Fortunately, we found that simultaneous mutations I102N and Y189A completely removed the oligomerization tendency of mEos2 and enhanced the brightness. This variant, which we termed mEos2-NA, behaved as a true monomer in gel filtration and ultracentrifuge analysis (**Supplementary Figs. 4** and **5**). mEos2-NA had very low homo-affinity with a dissociation constant (K_d) that was beyond the detection limit of our instrument (**Supplementary Table 2**), whereas the single mutants exhibited a moderate increase in K_d relative to that of mEos2 (20 μM).

One drawback of mEos2-NA was that it was not sufficiently bright. The lower extinction coefficient of mEos2-NA resulted in a 35% reduction in the brightness compared to green mEos2 (**Supplementary Table 2**). To improve the brightness of mEos2-NA, in a second round of protein optimization we mutated Ile157 and His158, which are near the chromophore and may contribute to the structure and brightness of the chromophore. Considering that the related residue of Ile157 in mKikGR is valine (**Supplementary Fig. 3**) and His158 is at the A–C interface, we used site-directed mutagenesis to change Ile157 to valine and His158 to charged residues; we identified two variants with substantially improved brightness that still retained monomeric properties (**Supplementary Table 3** and **Supplementary Figs. 1, 6** and **7**). These two variants, named mEos3.1 and mEos3.2, have I102N,I157V,H158E,Y189A and I102N,H158E,Y189A mutations, respectively, relative to mEos2 sequence.

As evidence of their monomeric property, mEos3.1 and mEos3.2 fused with Orai1 localized correctly to the plasma membrane (**Fig. 1a**). Moreover, the larger CRAC current (I_{CRAC}) of Orai1-mEos3.1 ($P = 1.17 \times 10^{-7}$) or Orai1- mEos3.2 ($P = 5.18 \times 10^{-8}$) relative to that of Orai1-mEos2 suggested that mEos3 variants minimally interfere with CRAC channel localization and function (**Fig. 1e**). We also fused mEos3.1 and mEos3.2 with several membrane proteins as well as intracellular markers and verified that these fusion proteins localized as expected (**Supplementary Figs. 2** and **8**). These results show that both mEos3.1 and mEos3.2 are excellent fusion partners for use in fluorescence microscopy.

In terms of the spectral properties, pK_a and photoconversion kinetics, both green and red form mEos3.1 and mEos3.2 were nearly identical to the precursor mEos2 (ref. 7) (**Supplementary Figs. 9–11** and **Supplementary Table 3**). However, purified mEos3.1 and mEos3.2 exhibited 1.55- or 1.13-fold greater brightness in the green form and comparable brightness in the red form to those forms of mEos2 (**Supplementary Table 3**). Moreover, mEos3.2 displayed the fastest maturation among other EosFP variants and mClavGR2 (a monomeric *Clavularia*-derived green-to-red photoconvertible protein), with a maturation half-time of 20 min (**Supplementary Fig. 12**). mEos3s displayed improved folding capability even when fused with a poorly folded target (**Supplementary Fig. 13**). As for photostability, mEos3.1 and mEos3.2 displayed similar photobleaching kinetics compared to that of mEos2 in the red states (**Supplementary Fig. 14**). After fusing mitochondria signal peptides with mEos3.2, we performed long-term mitochondria tracking and observed clear fragmentation in living HeLa cells (**Supplementary Fig. 15**), suggesting that mEos3.2 functions as an excellent monomer highlighter for long-term tracking experiments.

To test the performance of mEos3.1 and mEos3.2 in super-resolution imaging, we fused them with β-actin and α-actinin (**Supplementary Fig. 16**). We compared the total photon budget and localization precision of mEos3.1 and mEos3.2 with those of mEos2 fused with β-actin in HeLa cells. The total photon numbers of both

Table 1 | *In situ* photon statistics for mEos2, mEos3.1 and mEos3.2

β-actin–linked proteins	Number of molecules	Total photon number		Localization error (nm)	
		Mean	Median	Mean	Median
mEos2	335,820	382 ± 8	192 ± 2	15	13
mEos3.1	526,756	462 ± 16	243 ± 8	12	10
mEos3.2	885,985	482 ± 7	264 ± 7	12	10

The ± values indicate s.e.m. ($n = 5$ cells).

Figure 2 | Comparing the label density and Nyquist resolution of EosFP variants and mClavGR2. (**a**) Example PALM images of HeLa cells expressing Lifeact fused with mEos2, mEos3.1 and mEos3.2. Scale bars, 3 μm. (**b**) Distribution and cumulative ratio (inset) of label density for EosFP variants and mClavGR2. (**c**) Distribution of Nyquist resolution calculated from label density in **b**. (**d**) HeLa cells expressing Lifeact fused with mEos2 ($n = 14$) and mEos3.2 ($n = 10$) were randomly sampled, and the label density was analyzed. The average maximum ($P = 4.87 \times 10^{-12}$), mean ($P = 7.76 \times 10^{-10}$) and median ($P = 2.33 \times 10^{-6}$) label density of mEos3.2 were significantly larger than those of mEos2. P values were determined by Student's t-test. Error bars, s.e.m.
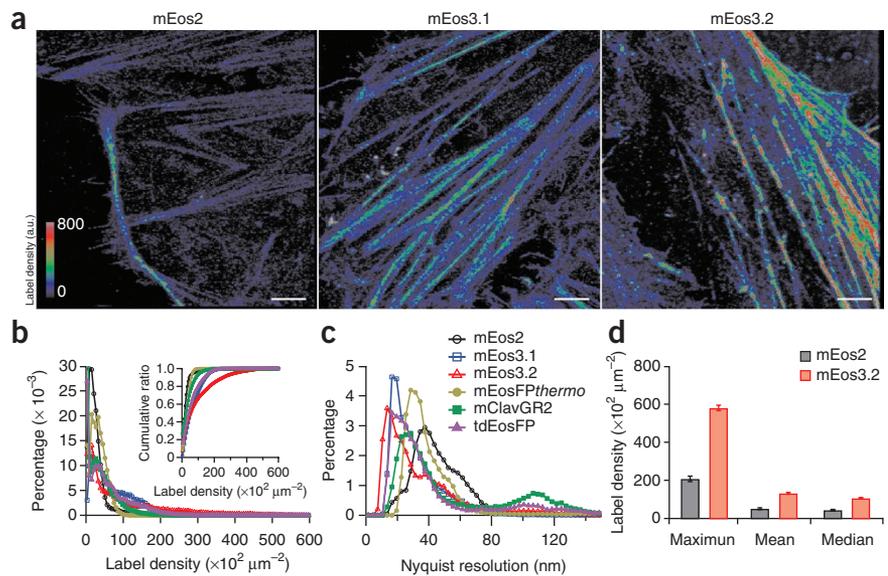
mEos3.1 and mEos3.2 were higher than those of mEos2. As a consequence, we calculated a higher localization precision for both mEos3.1 and mEos3.2 (**Table 1**). The spatial resolution of a super-resolution image is limited not only by the localization precision of each probe but also by the localization density in the structures. According to the Nyquist criterion, the average distance between neighboring localizations should be no more than half of the size of an object for the object to be resolvable. Therefore, a Nyquist resolution of $2/(\text{label density})^{1/D}$, where D is the dimension of the structure, must be considered when specifying the spatial resolution, in addition to the localization precision[13,14]. By fusing different PAFPs with Lifeact, a short peptide that binds actin[15], we compared their label densities in HeLa cells. mEos3.2 gave the highest label density (**Fig. 2a,b** and **Supplementary Table 4**) and hence higher Nyquist resolution than other EosFP variants and mClavGR2 (**Fig. 2c**). The maximum label density of mEos3.2 was approximately threefold higher of that of mEos2, which gave a 1.7-fold increase in Nyquist resolution (**Fig. 2c,d**). The higher label density of mEos3 variants was likely due to their better maturation and folding properties but not due to more photoblinking as they had slightly less blinking than mEos2 did (**Supplementary Fig. 17**).

In summary, we engineered two photoconvertible proteins, mEos3.1 and mEos3.2, based on the crystal structure of mEos2. As compared with other EosFP variants (mEosFP, mEosFP-thermo, tdEosFP and mEos2) and mClavGR2, mEos3.2 gives the best overall performance in brightness, maturation, monomericity, pH stability, photon budget after switching and label density (**Supplementary Table 5**). To our knowledge, mEos3.2 provides the highest label density and photon budget among all monomeric green-to-red PAFPs. Hence, mEos3.2 should be considered as a new probe to replace other EosFPs in both diffraction-limited and super-resolution microscopy.

METHODS

Methods and any associated references are available in the online version of the paper.

Accession code. Protein Data Bank: 3S05.

Note: Supplementary information is available in the online version of the paper.

AUTHOR CONTRIBUTIONS

M.Z., H.C., Y.Z., J.Y., W.J., J.C., B.L. and J.L. performed the research; L.W. and Y.L. assisted with data collection and solved the mEos2 structure; J.Z. assisted with spectrum measurement; M.Z., H.C., Y.Z., P.X. and T.X. analyzed data; T.X. and P.X. designed the research and wrote the paper.

1. Betzig, E. *et al. Science* **313**, 1642–1645 (2006).
2. Hess, S.T., Girirajan, T.P. & Mason, M.D. *Biophys. J.* **91**, 4258–4272 (2006).
3. Rust, M.J., Bates, M. & Zhuang, X. *Nat. Methods* **3**, 793–795 (2006).
4. Huang, B., Bates, M. & Zhuang, X. *Annu. Rev. Biochem.* **78**, 993–1016 (2009).
5. Wiedenmann, J. *et al. Proc. Natl. Acad. Sci. USA* **101**, 15905–15910 (2004).
6. Lippincott-Schwartz, J. & Patterson, G.H. *Trends Cell Biol.* **19**, 555–565 (2009).
7. McKinney, S.A., Murphy, C.S., Hazelwood, K.L., Davidson, M.W. & Looger, L.L. *Nat. Methods* **6**, 131–133 (2009).
8. Nienhaus, G.U. *et al. Photochem. Photobiol.* **82**, 351–358 (2006).
9. Hoi, H. *et al. J. Mol. Biol.* **401**, 776–791 (2010).
10. Zacharias, D.A., Violin, J.D., Newton, A.C. & Tsien, R.Y. *Science* **296**, 913–916 (2002).
11. Ando, R., Mizuno, H. & Miyawaki, A. *Science* **306**, 1370–1373 (2004).
12. Fuchs, J. *et al. Nat. Methods* **7**, 627–630 (2010).
13. Shroff, H., Galbraith, C.G., Galbraith, J.A. & Betzig, E. *Nat. Methods* **5**, 417–423 (2008).
14. Jones, S.A., Shim, S.H., He, J. & Zhuang, X. *Nat. Methods* **8**, 499–508 (2011).
15. Riedl, J. *et al. Nat. Methods* **5**, 605–607 (2008).

ONLINE METHODS

Plasmids. The genes encoding mEos2 and mEos3s were cloned into the BamHI and NotI sites of pEGFP-N1 (Clontech) and the NheI and BglII sites of pEGFP-C1 (Clontech) to replace the *EGFP* gene, which generated pmEos3-N1 and pmEos3-C1, respectively. The full-length *Homo sapiens H2B* (NCBI accession number BC005827) and *ACTN1* (BC003576) cDNAs with NheI and XhoI sites were PCR-amplified and inserted into pmEos3-N1. The cDNA of β-actin (*Homo sapiens*, NM_001101.3) was cloned into a pmEos3-C1 vector. To generate pmEos3-Mito, cDNAs of mEos3s containing AgeI and NotI sites were PCR-amplified and swapped with the HyPer gene in the pHyPer-dMito vector (Evrogen). *Src-N15* was fused to *mEos3.1* and *mEos3.2* sequences and inserted into the pEGFP-N1 vector with EcoRI and NotI sites. The mEos3s and mEos2 genes were cloned and inserted into the pTfR-EGFP-N1 plasmid using BamHI and NotI sites. To express Lifeact-fused fluorescent proteins in mammalian cells, the *Lifeact* sequence was cloned into pEGFP-N1 (Clonetech) with EcoRI and BamHI. And then cDNAs encoding mEos2, mEos3, mClavGR2 (ref. 9) (purchased from Allele Biotech), tdEosFP, mEosFP and mEosFP-thermo[16] (with an A69V mutation relative to mEosFP) containing BamHI and NotI sites were PCR-amplified and inserted in the plasmid to replace *EGFP*. Also, to label Orai1 (*Homo sapiens*, NM_032790.3), GRM4 (*Homo sapiens*, NCBI accession number NM_000841.2) and GLUT4 (*Mus musculus*, NM_009204.2) with PAFPs, the genes encoding mEos2, mEos3s and mEosFP-thermo were PCR-amplified and swapped with the *EGFP* gene in the vectors pOrai1-EGFP-N1, pCDNA5-GRM4-EGFP and pGLUT4-EGFP-N1 (ref. 17) using BamHI and NotI. To construct prokaryotic expression vectors, pRSETa-mEos2 (Addgene plasmid 20341) was double-digested by EcoRI and BamHI and PCR-amplified genes encoding EosFP and mClavGR2 were inserted. The primer sequences are listed in **Supplementary Table 6**.

Generation of bright, monomeric mEos3 variants. All mutants were generated by performing site-directed mutagenesis on pRSETa-mEos2. Sequencing-verified clones were then transformed into BL21(DE3)pLysS (Novagen) *Escherichia coli* to overexpress proteins. To screen for monomeric proteins, purified proteins with good performance in gel filtration were selected to perform analytical ultracentrifuge assays using a sedimentation equilibrium method. For brightness screening, purified proteins' fluorescence quantum yields and extinction coefficients were calculated as described below.

Protein expression and purification. The EosFP proteins, mClavGR2 and mEos3 proteins were expressed in the *Escherichia coli* strain BL21(DE3)pLysS and purified using a Ni-NTA His-Bind resin (Qiagen), followed by a gel-filtration step using a Superdex 200 column (GE Healthcare). For additional analysis, purified proteins were concentrated by ultrafiltration and diluted in PBS.

Crystallization and structure determination. The green-form mEos2 protein (10 mg/ml) was crystallized in the absence of light at 16 °C in 0.2 M magnesium chloride hexahydrate, 0.1 M Tris pH 8.5 and 25% w/v polyethylene glycol 3350 in hanging drops. The crystals were then transferred to cryosolvent and flash-frozen in liquid nitrogen before X-ray structure analyses. Diffraction data were collected at BL-5A at PF Tsukuba and then integrated and scaled using HKL2000. Phase information was obtained by molecular replacement with the program Phaser using coordinates of the green-form EosFP (PDB identifier 1ZUX), which has 96% sequence identity to mEos2. The model was completed using the program COOT (Crystallographic Object-Oriented Toolkit) and iteratively refined using PHENIX.refine. The final model was obtained with an *R* factor of 0.151 and free *R* factor of 0.216.

Analysis of oligomerization. Size-exclusion chromatography was first performed using a Superdex 200 column and an Akta purifier system (GE Healthcare) to check the oligomeric states of all variants. Before chromatography, proteins were concentrated to 3–4 mg/ml. The flow rate was set to 0.5 ml/min. Protein absorption was monitored at 280 nm. All measurements were performed at 16 °C. The elution volume was compared between all mutants and mEos2, and those that appeared to have smaller molecular weights were selected for analytical ultracentrifuge assays. Sedimentation equilibrium experiments were performed on a Beckman Optima XL-I analytical ultracentrifuge at 20 °C as previously described[10]. Purified proteins at 8 to 20 μM were loaded into 6-channel centrifugation cells and normalized to the corresponding dialysis buffer (PBS pH = 7.4). Samples were centrifuged at 10,000 r.p.m., 15,000 r.p.m. and 20,000 r.p.m. sequentially. The data were analyzed by nonlinear least-squares analysis using the software package (Microcal Origin) supplied by Beckman. The solvent density, partial specific volume and calculated molecular weight used in the analysis were determined by Sedenterp v 1.01 and listed in **Supplementary Table 7**.

Protein characterization. Proteins were first diluted in PBS to limit UV-light absorption to less than 0.1 so that quantum yields could be accurately measured. The absorption and excitation and emission spectra were then immediately recorded using an Agilent 8453 UV-visible spectrophotometer and an Edinburgh Instrument FLS920, respectively. For the emission spectra, mEos3 were irradiated with 503 nm (573 nm for the red form) light. To determine the fluorescence excitation spectra, fluorescence was recorded at 513 nm (580 nm for the red form). Fluorescence quantum yields and the molar extinction coefficients at the respective absorption maxima of the green form were determined relative to the reported value for mEos2 (quantum yield, 0.84; molar extinction coefficient at 506 nm, 56,000 M^{-1} cm^{-1})[7]. For red-form fluorescence, rhodamine (quantum yield, 0.65) in alcohol was used as the reference for calculating quantum yields at 550 nm, and the molar extinction coefficients at 570 nm were determined by a comparison between the absorbance decrease in the green forms and the increase in the red forms, as previously described[18,19].

pK_a and maturation data were obtained in a Varioskan Flash spectral scanning multimode reader (Thermo Scientific) with 96-well optical bottom plates (Nunc). For pK_a measurements, purified mEos3 was diluted in buffers with various pH values that ranged from 3 to 11; the emission fluorescence at 518 nm and 525 nm (585 nm and 590 nm for the red form) were immediately recorded, and the values were averaged. The pK_a value was taken as the pH value where the fluorescence reached 50% of the maximum. To determine the chromophore maturation time of mEos3, the purified proteins were mixed in denaturation buffer (8 M urea and 1 mM DTT), then heated to 95 °C for 5 min and diluted 100× into renaturation buffer (35 mM KCl, 2 mM $MgCl_2$,

50 mM Tris pH 7.5 and 1 mM DTT); fluorescence at 525 nm was subsequently monitored at 37 °C.

Cell culture and transfection. HEK293 cells, HeLa cells, COS-7 cells and BS-C-1 cells were cultured in Dulbecco's Modified Eagle Medium (DMEM) complete medium (Gibco) supplemented with 10% FBS and maintained at 37 °C and 5% CO_2 in a humidified incubator. Cells were then transiently transfected using Lipofectamine 2000 (Invitrogen) in accordance with the manufacturer's protocol. After transfection, the cells were grown in DMEM complete medium for 24 h. For PALM imaging, cells were grown in improved minimum essential medium (IMEM; Gibco) or DMEM complete medium without phenol red.

Confocal microscopy and cell imaging. Confocal microscopy images of mEos3 were obtained using an FV500 laser-scanning confocal microscope (Olympus). All the figures were produced using a 60×, 1.4 numerical aperture (NA) oil-immersion objective. The maximum power near the rear pupil of the objective was 0.18 mW for the 405-nm laser (LASOS), 0.24 mW for the 488-nm laser and 0.08 mW for the 561-nm laser. Images were quantified and analyzed using FluoView software (Olympus) and ImageJ (US National Institutes of Health).

Determination of photoconversion rate. HEK293 cells were transiently transfected in culture medium with purified plasmids encoding untagged mEos2, mEos3.1 and mEos3.2. After 24 h of incubation, the cells were transferred to cover glasses (Fisher) for an additional 24 h before imaging. All photoconversion measurements were obtained using an FV500 laser scanning confocal microscope with an Olympus 60× 1.4 NA oil-immersion objective. The 543 nm laser power was constant at 0.012 mW with increasing 405 nm activation intensity in the range of 0.01–0.16 mW.

Photobleaching decay kinetics. Photobleaching experiments used HeLa cells transfected with purified plasmids encoding H2B-mEos2, H2B-mEos3.1 and H2B-mEos3.2, as previously described[20]. We used an FV500 laser-scanning confocal microscope of the same laser power (488-nm laser: 24 μW; 543-nm laser: 64 μW) for comparison and collected green and red fluorescence signals in two channels spanning 500–522 nm (488-nm laser) and 550 nm long-pass (543-nm laser). A 405-nm laser was used to photoconvert the protein.

Measurement of I_{CRAC}. Patch clamp experiments were performed at room temperature using the standard whole-cell recording configuration as previously described[21–23]. Cells were plated on poly(L-lysine)-coated cover slips 12–24 h before experiments. The extracellular solution contained 140 mM cesium glutamate, 6 mM $CaCl_2$, 2 mM $MgCl_2$, 10 mM tetraethylammonium chloride and 10 mM HEPES (pH = 7.4, adjusted with CsOH). For recording constitutive I_{CRAC}, the pipette was filled with a solution containing 140 mM cesium glutamate, 8 mM $MgCl_2$, 10 mM BAPTA, 3.5 mM $CaCl_2$ and 10 mM HEPES (pH = 7.2, adjusted with CsOH). The free $[Ca^{2+}]$ of this solution was calculated to be 145 nM using MaxChelator. Before patch-clamp recording, the green (mEos2, mEos3.1 or mEos3.2) fluorescence of each cell was excited by a xenon light source at 488 nm and measured at

510 nm ± 5 nm with a photodiode; simultaneously, the red (mKO) fluorescence was excited at 561 nm and measured at 610 nm ± 20 nm. After establishment of the whole-cell configuration, voltage stimuli that consisted of a 10 ms step to −100 mV followed by a 50 ms voltage ramp from −100 mV to +100 mV were delivered from the holding potential of 0 mV every 2 s. Currents were digitized at a rate of 20 kHz and filtered offline at 2.9 kHz. All current traces were leak-subtracted. The current curves collected by delivering voltage ramps after gigaohm seal formation and break-in, but not eliciting CRAC current, were assigned as leak current. Capacitive currents were determined and corrected before each voltage ramp. The current amplitudes at −100 mV of the individual ramps were used for statistical analysis. Data were analyzed by IGOR Pro 5.01 (Wavemetrics). Averaged results were presented as the mean values ± s.e.m. with the numbers of experiments indicated.

PALM setup and data analysis. PALM imaging of mEos2, mEos3.1 and mEos3.2 was performed as previously described[1]. We used an Olympus IX71 inverted microscope equipped with a 100×, 1.45 NA oil objective (Olympus PLAN APO). The fluorescence signals were acquired using an electron-multiplying charge-coupled device (EMCCD) camera (Andor iXon DV-897 BV). The maximum power near the rear pupil of the objective was 8.74 mW for the 405-nm laser (LASOS), 4.13 mW for the 491-nm laser (Cobolt Dual Calypos) and 2.54 mW for the 561-nm laser (Cobolt Jive). The intensity of the 405-nm laser was set so that it only activated a few molecules in each frame. Data analysis and super-resolution image reconstruction were performed as previously described[1,21,24]. Briefly, a wavelet transform algorithm[25] with a proper threshold was used for single-molecule detection, and localizations of the molecules were determined by finding local maxima with a mask of 5 × 5 pixels. Then the raw images of molecules in the fit windows (7 × 7 pixels) were background-subtracted, and the pixel values were converted to numbers of photons. After that, all molecules were fitted with a 2D Gaussian using MLE_GPU algorithm[26] to obtain the number of photons (N) and the s.d. of the point spread function (s). The background noise per pixel (b) was determined by taking the s.d. of the intensity (in photons) of an illuminated area in a raw image where no single molecule is visible. Finally, the 2D localization precision for each molecule was calculated according to the following equation[27]:

$$\sigma^2 = \frac{S^2 + \alpha^2/12}{N} + \frac{8\pi S^4 b^2}{\alpha^2 N^2} \qquad (1)$$

Single-molecule immobilization in PAA layer for photoblinking experiment. mEos2, mEos3.1 and mEos3.2 were purified as described above and diluted to 10^{-8}– 10^{-10} M in Tris-HCl (pH = 7.5). To immobilize the molecules, 42 μl of diluted protein solution with 0.1 μm TetraSpeck microspheres (Invitrogen) was mixed with 30 μl of acrylamide, 0.5 μl of 10% TEMED and 0.5 μl of 10% ammonium persulfate[28]. First, two cleaned cover slips were prepared. Second, 10 μl of mixed buffer was placed at the center of one cover glass, and the other cover glass was quickly pressed on it to obtain a 1 μl thin layer. After complete polymerization, the samples were placed in a chamber and imaged using the same setup as PALM. Blinking analysis was performed as previously

described[29,30] except that the radius is set to 100 nm. Besides, we used fluorescent beads as fiducial markers for drift correction, which largely reduced the influence of sample drift.

Label density and Nyquist resolution analysis. We selected the same size (24 μm × 32 μm, which contains most area of a cell) from each image and calculated the density of each position where single molecule exists. The Nyquist resolution was computed according to the equation as previously described[4].

16. Wiedenmann, J. *et al. J. Biophotonics* **4**, 377–390 (2011).
17. Bai, L. *et al. Cell Metab.* **5**, 47–57 (2007).
18. Chudakov, D.M. *et al. Nat. Biotechnol.* **22**, 1435–1439 (2004).

19. Subach, O.M. *et al. Nat. Methods* **8**, 771–777 (2011).
20. Shaner, N.C. *et al. Nat. Methods* **5**, 545–551 (2008).
21. Ji, W. *et al. Proc. Natl. Acad. Sci. USA* **105**, 13668–13673 (2008).
22. Li, Z. *et al. J. Biol. Chem.* **282**, 29448–29456 (2007).
23. Xu, P. *et al. Biochem. Biophys. Res. Commun.* **350**, 969–976 (2006).
24. Shroff, H. *et al. Proc. Natl. Acad. Sci. USA* **104**, 20308–20313 (2007).
25. Olivo-Marin, J.C. *Pattern Recognit.* **35**, 1989–1996 (2002).
26. Smith, C.S., Joseph, N., Rieger, B. & Lidke, K.A. *Nat. Methods* **7**, 373–375 (2010).
27. Thompson, R.E., Larson, D.R. & Webb, W.W. *Biophys. J.* **82**, 2775–2783 (2002).
28. Grotjohann, T. *et al. Nature* **478**, 204–208 (2011).
29. Annibale, P., Scarselli, M., Kodiyan, A. & Radenovic, A. *J. Phys. Chem. Lett.* **1**, 1506–1510 (2010).
30. Annibale, P., Vanni, S., Scarselli, M., Rothlisberger, U. & Radenovic, A. *Nat. Methods* **8**, 527–528 (2011).